







Open Archive Toulouse Archive Ouverte (OATAO)

OATAO is an open access repository that collects the work of Toulouse researchers and makes it freely available over the web where possible

This is an author's version published in: <http://oatao.univ-toulouse.fr/23660>

Official URL: <https://doi.org/10.1016/j.corsci.2013.07.041>

To cite this version:

Tan, Xipeng and Perrin-Pellegrino, Carine and Hoummada, Khalid and Mangelinck, Dominique and Vande Put, Aurélie  and Lafont, Marie-Christine  and Oquab, Djar  and Monceau, Daniel  *Atom probe tomographic study of L10 martensite in a Pt-modified NiCoCrAlYTa bond coating.* (2013) Corrosion Science, 76. 1-5. ISSN 0010-938X

Any correspondence concerning this service should be sent to the repository administrator: tech-oatao@listes-diff.inp-toulouse.fr

Letter

Atom probe tomographic study of L1₀ martensite in a Pt-modified NiCoCrAlYTa bond coating

Xipeng Tan^{a,*}, Carine Perrin-Pellegrino^a, Khalid Hoummada^a, Dominique Mangelinck^a, Aurélie Rouaix Vande Put^b, Marie-Christine Lafont^b, Djar Oquab^b, Daniel Monceau^b

^aIM2NP, UMR 7334 CNRS, Université Aix-Marseille, Av Escadrille Normandie-Niemen, Case 142, 13397 Marseille Cedex 20, France

^bInstitut Carnot CRIMAT, ENSIACET, 4, allée Emile Monso, BP 44362, 31030 Toulouse Cedex 4, France

ARTICLE INFO

Keywords:

A. Metal coating

B. TEM

C. Segregation

ABSTRACT

The L1₀ martensite formed in a Pt modified NiCoCrAlYTa bond coating has been investigated by atom probe tomography. It was found that obvious segregation of Co and Cr occurred in the micro twins zone inside the martensite lath. Based upon the compositional analysis, it is known that Pt destabilizes the β phase and Co and Cr act as β stabilizers with respect to the $\beta \rightarrow$ L1₀ martensitic transformation. In addition, some α Cr particles precipitated inside the martensite lath.

1. Introduction

MCrAlY type overlay coatings (M = Ni and/or Co) are used as bond coatings in the four layered thermal barrier coating (TBC) system (i.e. (i) the superalloy substrate, (ii) the bond coat, (iii) the thermally grown oxide (TGO), and (iv) the ceramic top coat) as they provide superior oxidation and corrosion resistance for hot section components in gas turbine engines [1–3]. They are capable of bonding the yttria stabilized zirconia (YSZ) top coat and superalloy substrate. Many studies have addressed the microstructural characterization of TBC multi layered systems [4–7]. Moreover, the oxidation [8] and hot corrosion [9,10] behaviour of MCrAlY type coating or TBC systems have been widely investigated. It is well known that each element in the MCrAlY coatings would play different roles, e.g., Ni acts as the matrix, Co stabilizes β and γ phases, Al is responsible for aluminum oxide (α Al₂O₃) formation to protect the system against oxidation, Cr provides corrosion resistance and helps the formation of alumina (“third element effect”), Y is beneficial for TGO adherence, etc. [11,12]. In addition, Pt was intentionally deposited on the external surface of MCrAlY coatings to obtain improved oxidation and corrosion resistance in practical use [13].

Recently, the benefit of Pt on MCrAlY coatings has received increasing interest. Vande Put et al. [14,15] studied the effect of Pt on the microstructure and oxidation resistance of NiCoCrAlYTa coatings manufactured by different processes. Herein, L1₀

martensite appeared in the external zone of Pt modified NiCoCrAlYTa coatings after fabrication. This martensite phase formed a continuous layer in the case of vacuum plasma sprayed NiCoCrAlYTa and a discontinuous but dense layer in the case of electrolytic NiCoCrAlYTa. This layer formation was explained by the uphill diffusion of Al during the heat treatment after the electrolytic deposition of Pt [14]. As observed in Ni rich β NiAl phase (B2 structure), this phase will undergo a martensitic transformation during cooling [16]. It is referred to the L1₀ or 3R martensite with face centered tetragonal (fct) lattice. Moreover, the reverse transformation from martensite to β phase occurs upon heating. This martensitic transformation has been commonly observed in β NiAl [17,18] or Pt modified β NiAl bond coatings when Al was depleted by interdiffusion and alumina scale spallation and reforming [19–22]. The volume change associated with this transformation in Pt modified β NiAl lies between 1% [19] and 1.9% [16] depending on composition. In Pt modified aluminide coatings, this volume change can favor bond coating surface rumpling which is detrimental to the thermal barrier system durability [23].

Furthermore, several studies have shown the martensitic transformation in MCrAlY coatings, which contain a volume fraction of β NiAl, during thermal cycling [24,25]. Multiply twinned configurations are widely recognized as the most important structural features of L1₀ martensite [26]. Numerous papers have reported the occurrence of micro twins in the martensite laths in NiAl bond coatings or related NiAl alloys [19,27,28]. Liang et al. [29] observed the B2 \rightarrow L1₀ martensitic transformation and the macro twinned martensite plates as well as large numbers of micro twins inside each plate in a model NiCrAlY alloy. It is believed that the

* Corresponding author. Tel.: +33 0667416065.

E-mail address: xptan1985@gmail.com (X. Tan).

Table 1
Nominal composition of the alloy AM3.

		Ni	Al	Cr	Co	Ta	Ti	Mo	W
AM3	wt.%	Bal.	6.0	8.0	6.0	4.0	2.0	2.0	5.0
	at.%	Bal.	12.85	8.89	5.88	1.28	2.41	1.20	1.57

micro twin planes could accommodate the constant shear of the martensitic transformation, i.e. the habit plane stress, which exists due to the small twin surface energy of NiAl parent phase [30]. Therefore, the high density of micro twins in martensitic micro structures is of great concern during the transformation process. It is noted that the L1₀ martensite has been extensively studied both on crystallography and chemistry with the aid of transmission electron microscopy (TEM). However, it still lacks of quantitative chemical characterization on the L1₀ martensite, especially for the sub microstructures inside the martensite laths. Atom probe

tomography (APT) is the unique and powerful technique, which is able to locate the alloying elements and quantify the composition at the atomic scale and in the three dimensions [31,32]. This should allow a more detailed understanding of the martensitic transformation and any alloying effects.

This work presents the chemical analysis of micro twins in the martensite lath by utilizing APT, with the goal of studying the solute redistribution among these sub microstructures as well as the effect of alloying elements on the formation of L1₀ martensite.

The NiCoCrAlYTa coating was deposited on the first generation Ni based superalloy AM3 (see its composition in Table 1) by vacuum plasma sprayed (VPS) at the LERMPS laboratory (Sévenans, France). The AMDRY powder with a composition of Ni 23Co 20Cr 8.5Al 4Ta 0.6Y (wt.%) or Ni 20.9Co 20.9Cr 16.9Al 1.2Ta 0.4Y (at.%) was employed for the NiCoCrAlYTa deposition. In order to reduce the roughness resulting from the VPS process, P1200 SiC paper was used to partially polish the NiCoCrAlYTa surface. Polishing would be terminated once a "partially machined" surface

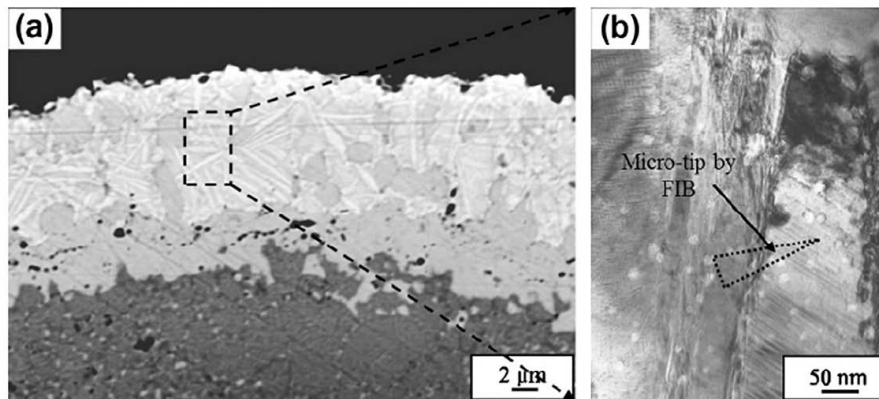


Fig. 1. (a) BSE image showing the cross-section of the outer part of the Pt-modified NiCoCrAlYTa bond coating. (b) TEM bright field image showing a martensite lath in (a).

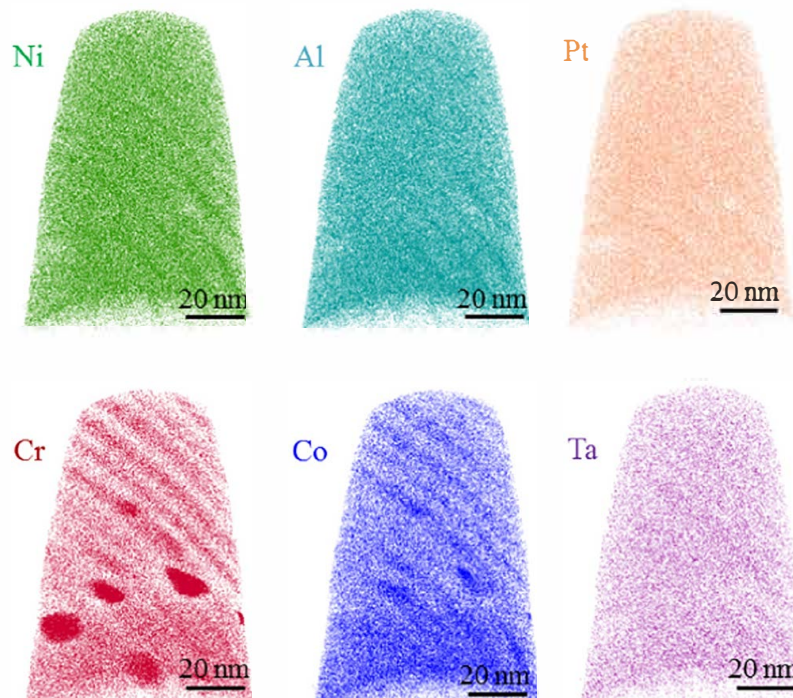


Fig. 2. APT reconstruction ($80 \times 80 \times 110 \text{ nm}^3$) showing the atom maps of Ni (Green), Al (light blue), Pt (Orange), Cr (Red), Co (Blue) and Ta (Purple). (For interpretation of the references to color in this figure legend, the reader is referred to the web version of this article.)

(namely between 24% and 34% of polished surface) was obtained, which was estimated by means of optical microscopy and image analysis. After the partial polishing, Pt was deposited by sputtering at Cranfield University (England). The NiCoCrAlYTa coating was 70–80 μm . The thickness of Pt layer was 7 μm with an uncertainty of $\pm 1 \mu\text{m}$. Moreover, heat treatment was carried out for 6 h at 1080 $^{\circ}\text{C}$ under vacuum after Pt deposition.

Scanning electron microscopy (SEM) observations of bond coating cross sections were performed by a LEO 435VP microscope using the backscattered electron (BSE) mode. For the transmission electron microscopy (TEM) sample preparation, cross sections were taken from the “superalloy + bond coating” systems using a diamond wire saw. The two thin slices of sample were glued coating against coating with epoxy resin, and embedded in a 3 mm diameter brass tube. After curing, the tube was sectioned into approximately 300 μm thick discs. The disc was then polished on both sides and dimpled before ion milling to transparency with a Gatan precision ion polishing system. The disc was observed periodically during the thinning processes to ensure that the hole was approximately located across the interface of interest. TEM observations of the thin foil were carried out using a JEOL JEM 2010 microscope operating at 200 kV. APT specimens were prepared by focused ion beam (FIB) on a FEI Helios dual beam via the lift out technique [33]. The micro tips were prepared by means of the annular milling method [34] to obtain an end radius of $\sim 100 \text{ nm}$. APT analyses were performed with an Imago Scientific Instruments LEAP 3000 \times HR at a specimen temperature of 55 K, a 100 kHz picosecond laser pulses with an energy of 0.2 nJ, an evaporation rate of 0.002 ions pulse $^{-1}$ and a pressure of

$< 2 \times 10^{-11}$ Torr. Data reconstruction was performed using IVASTM 3.6.2 software.

Fig. 1a shows the cross section microstructure of this Pt modified NiCoCrAlYTa bond coating. Because Pt is a heavy metal, the outer “brighter” part should be considered as the Pt affected zone under the BSE mode. In particular, numerous martensite laths with the brightest contrast were clearly observed in the Pt affected zone. These laths have been identified as the $L1_0$ martensite in Ref. [14]. One of the martensite laths is shown in Fig. 1b. It reveals that a large number of micro twin bands exist inside the martensite lath. In addition, many small precipitates were also present both inside and outside the martensite lath. The tip for APT analysis was taken from the position as illustrated in Fig. 1b. Fig. 2 reveals the atom maps in the 3 dimensional APT reconstruction volume, which consists of three different regions, i.e. the lamellar segregation region (at top), the irregular Cr rich particles region (in the middle) and the chemical homogeneous region (at bottom). Lamellar structures were apparently observed. The average thickness of these segregation layers is determined as $6.2 \pm 0.7 \text{ nm}$ in terms of the APT reconstruction, which is in good agreement with the width of micro twins inside the martensite lath (as shown in Fig. 1b). Here, Cr and Co exhibit the most obvious segregation. In addition to these six elements in Fig. 2, a trace amount of Ti was also detected in the APT volume. Ti is expected to originate from the superalloy substrate via diffusion during the deposition of coating and the subsequent heat treatment. However, the only one isotope of element Y was not detected in the mass spectrum, either in the singly and doubly charged state or molecular ions. That may be due to the fact that most of the Y was bonded to

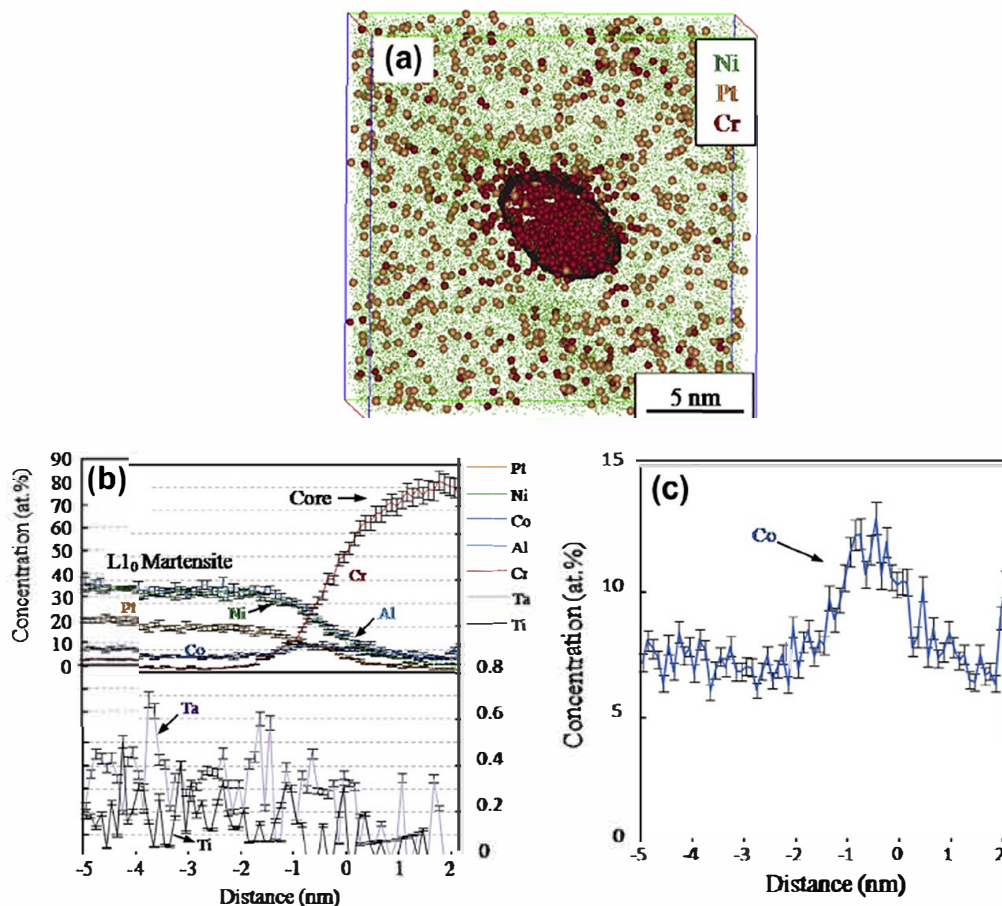


Fig. 3. (a) Selected portion of APT reconstruction showing the Cr-rich particle delineated with the 50 at.% Cr iso-concentration surface. (b) Proximity histogram (proxigram) showing the concentration profiles across the above interface. (c) Enlarged concentration profile for Co in (b).

oxygen and preferentially enriched at the splat boundaries inside the coating after deposition [35]. Moreover, several Cr rich particles were seen in the reconstruction volume of Cr atom map.

Fig. 3a shows the reconstructed Cr rich precipitate. Due to the local magnification effect [36], it is difficult to resolve any atomic planes. Concentration profiles for each atom obtained from proximity histogram (proxigram) analysis are shown in Fig. 3b. This proxigram was created using 0.1 nm bin size with respect to a 50 at.% iso concentration reference surface. It can be seen that the core region of the precipitate contains up to 80.0 ± 2.0 at.% Cr. Thus, it is α Cr phase. This phase forms next or in β NiAl phase during cooling because Cr solubility in β phase is low and decreases when temperature decreases. In addition, it is transparent that Co was segregated at the martensite/ α Cr heterophase interface. The Gibbsian interfacial excess of an element i , Γ_i , is defined by the excess number of solute atoms i (N_i^{excess}) per unit area (A). Γ_i can be determined utilizing proxigram concentration profiles for an arbitrary interface by [37,38]:

$$\Gamma_i = \frac{N_i/A}{\rho \Delta x} \sum_{j=1}^p (c_i^j - c_i^m) \quad (1)$$

where ρ is the atomic density ($97.39 \text{ atoms nm}^{-3}$ for the $L1_0$ martensite), Δx is the distance between the p layers in the proxigram, c_i^j is the concentration of the j th atom, and c_i^m is the average concentration of element i in the matrix. In terms of the proxigram in Fig. 3c, Co segregated with a Γ_i value of $8.41 \pm 0.46 \text{ atoms nm}^{-2}$.

In order to analyze the elemental segregation in the martensite lath, an 18 at.% Cr and Co iso concentration surface is shown in Fig. 4a. According to the location of APT sample, it can be known

that the bottom region is the β NiAl phase. Therefore, Cr and Co are known to homogeneously disperse in the β phase. As shown in Fig. 4b, $L1_0$ martensite contains less Cr and Co in comparison with the β phase. On the contrary, more Pt appears in the martensite, which results in the brightest contrast of martensites in the BSE image. It is noted that the concentrations of Ni and Al are almost identical (~ 35 at.%) in the martensite. Fig. 4c reveals the wave like concentration profiles for Ni, Al, Pt, Co and Cr. The concentration variations follow similar trends for each respective element. It is evident that these lamellar segregation zones correspond to the large number of micro twins inside the martensite lath. It has been known that the martensitic transformation only occurs in Ni rich NiAl alloys when some requirements are satisfied in Ni rich binary NiAl alloys, e.g., less than 37 at.% of Al content, higher than ~ 1000 °C of exposure temperature and sufficiently fast cooling rate [18]. Furthermore, the martensitic transformation is known to take place in the vicinity of the $\text{Ni}_{65}\text{Al}_{35}$ composition based upon the Ni-Al binary phase diagram and the excess Ni was randomly distributed on the Al sublattice [26]. In the present work, the concentration of Al in martensite has been determined as 35.0 ± 0.5 at.% (see Fig. 4b). Cr was suggested to predominately occupy the Al sublattice [39]. Moreover, Pt preferentially partitions to Ni sites [28]. Hence, the martensitic transformation was able to occur under the depleted Ni condition when cooled down from 1080 °C heat treatment in this work. Referring to the concentration profile of Al in Fig. 4c, its peak value was exactly ~ 35 at.%. While its valley concentration was down to ~ 30 at.%. It indicates that the regions with the enrichment of Ni, Al and Pt and depletion of Co and Cr represent the martensite. Since the martensitic transformation is

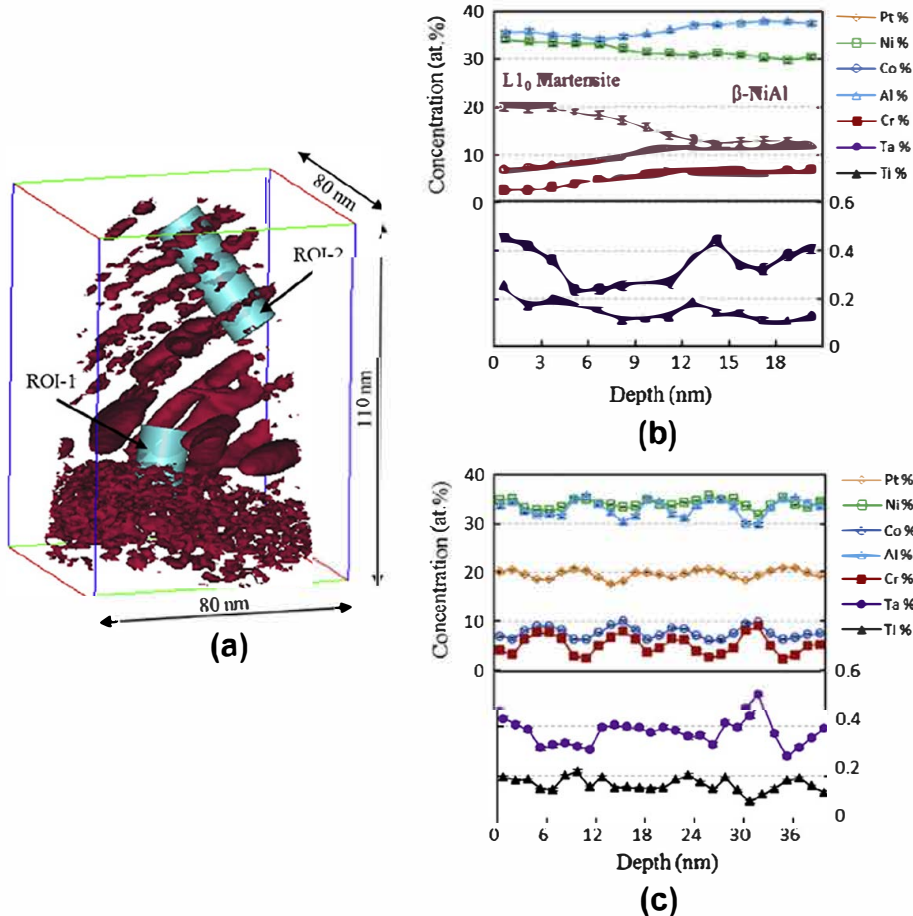


Fig. 4. (a) APT reconstruction showing the 18 at.% (Cr + Co) iso-concentration surface. (b) 1-dimensional concentration profiles for each atomic species obtained from the region of interest (ROI)-1 in (a). (c) 1-dimensional concentration profiles for each atomic species obtained from ROI-2 in (a).

extremely sensitive to the Al concentration, it was speculated that Cr and Co might be segregated at the micro twins of retained β parent phase. However, it still requires more work to verify this segregation phenomenon.

As the chemical analysis of martensite and β phase stated above, it was found that Pt destabilizes the β phase, i.e. promotes the martensitic transformation. By contrast, Co and Cr would stabilize the β phase. Additionally, Pt and Co appear to have the higher solubility both in β phase and martensite compared to Cr. As the martensitic transformation proceeds, it is possible to imagine that Cr was continuously ejected from the forming martensite and then aggregated to form the α Cr precipitates.

2. Conclusion

In summary, APT has been employed to analyze the sub micro structures of $L1_0$ martensite lath formed in a Pt modified NiCoCrAlYTa bond coating. It was found that there exists obvious segregation of Co and Cr in the micro twins zone inside the martensite lath. According to the compositional analysis of martensite and β phase, it is known that Pt destabilizes the β phase. However, Co and Cr act as β stabilizers with respect to the $\beta \rightarrow L1_0$ martensitic transformation. In addition, some α Cr precipitated inside the martensite lath. Co was found to segregate at the $L1_0/\alpha$ heterophase interface with a Gibbsian interfacial excess of 8.41 ± 0.46 atoms nm^{-2} . The chemical information at the atomic scale obtained by APT is a good supplementary for understanding the $L1_0$ martensitic transformation only utilizing TEM techniques.

References

- [1] R.A. Miller, Surf. Coat. Technol. 30 (1987) 1–11.
- [2] R.A. Miller, J. Therm. Spray. Technol. 6 (1997) 35–42.
- [3] N.P. Padture, M. Gell, E.H. Jordan, Science 296 (2002) 280–284.
- [4] A. Rabiei, A. Evans, Acta Mater. 48 (2000) 3963–3976.
- [5] Z.H. Zhou, H.B. Guo, J. Wang, M. Abbas, S.K. Gong, Corros. Sci. 53 (2011) 2630–2635.
- [6] X.P. Tan, H.U. Hong, B.G. Choi, I.S. Kim, C.Y. Jo, T. Jin, Z.Q. Hu, J. Mater. Sci. 48 (2013) 1085–1089.
- [7] H.U. Hong, J.G. Yoon, B.G. Choi, I.S. Kim, C.Y. Jo, Scripta Mater. 69 (2013) 33–36.
- [8] F.H. Yuan, Z.X. Chen, Z.W. Huang, Z.G. Wang, S.J. Zhu, Corros. Sci. 50 (2008) 1608–1617.
- [9] K. Zhang, M.M. Liu, S.L. Liu, C. Sun, F.H. Wang, Corros. Sci. 53 (2001) 1990–1998.
- [10] H. Mei, Y.N. Liu, L.F. Cheng, L.T. Zhang, Corros. Sci. 55 (2012) 201–204.
- [11] A. Nicoll, G. Wahl, Thin Solid Films 95 (1982) 21–34.
- [12] R. Sivakumar, B. Mordike, Surf. Coat. Technol. 37 (1989) 139–160.
- [13] J.R. Nicholls, JOM 52 (2000) 28–35.
- [14] A. Vande Put, M.-C. Lafont, D. Oquab, A. Raffaitin, D. Monceau, Surf. Coat. Technol. 205 (2010) 717–727.
- [15] A. Vande Put, D. Oquab, E. Péré, A. Raffaitin, D. Monceau, Oxid. Met. 75 (2011) 247–279.
- [16] D.J. Sordelet, M.F. Besser, R.T. Ott, B.J. Zimmerman, W.D. Porter, B. Gleeson, Acta Mater. 55 (2007) 2433–2441.
- [17] S. Rosen, J.A. Goebel, Trans. TMS-AIME 242 (1968) 722–724.
- [18] J.L. Smialek, Metall. Trans. 2 (1971) 913–915.
- [19] Y. Zhang, J. Haynes, B. Pint, I. Wright, W. Lee, Surf. Coat. Technol. 163 (2003) 19–24.
- [20] M. Chen, R. Ott, T. Hufnagel, P. Wright, K. Hemker, Surf. Coat. Technol. 163 (2003) 25–30.
- [21] M. Chen, M. Glynn, R. Ott, T. Hufnagel, K. Hemker, Acta Mater. 51 (2003) 4279–4294.
- [22] N. Vialas, PhD thesis, Institut National Polytechnique de Toulouse, 2004.
- [23] D.S. Balint, J.W. Hutchinson, J. Mech. Phys. Solids 53 (2005) 949–973.
- [24] B. Mendis, B. Tryon, T. Pollock, K. Hemker, Surf. Coat. Technol. 201 (2006) 3918–3925.
- [25] B. Mendis, K. Hemker, Scripta Mater. 58 (2008) 255–258.
- [26] D. Schryvers, B. De Saegher, J. Van Landuyt, Mater. Res. Bull. 26 (1991) 57–66.
- [27] D. Schryvers, P. Boullay, P.L. Potapov, R.V. Kohn, J.M. Ball, Int. J. Solids Struct. 39 (2002) 3543–3554.
- [28] M. Clancy, M.J. Pomeroy, C. Dickinson, J. Alloys Compd. 523 (2012) 11–15.
- [29] J.J. Liang, H. Wei, Y.L. Zhu, T. Jin, X.F. Sun, Z.Q. Hu, Surf. Coat. Technol. 206 (2012) 2746–2750.
- [30] D. Schryvers, Y. Ma, J. Alloys Compd. 221 (1995) 227–234.
- [31] K. Houmada, I. Blum, D. Mangelinck, A. Portavoce, Appl. Phys. Lett. 96 (2010) (1906) 261904–261926.
- [32] D. Mangelinck, K. Houmada, A. Portavoce, C. Perrin, R. Daineche, M. Descoins, D.J. Larson, P.H. Clifton, Scripta Mater. 62 (2010) 568–571.
- [33] K. Thompson, D. Lawrence, D. Larson, J. Olson, T. Kelly, B. Gorman, Ultramicroscopy 107 (2007) 131–139.
- [34] D. Larson, D. Foord, A. Petford-Long, H. Liew, M. Blamire, A. Cerezo, G. Smith, Ultramicroscopy 79 (1999) 287–293.
- [35] S.C. Vergel, C. Kwakernaak, T.J. Nijdam, W.G. Sloof, Mater. High Temp. 26 (2009) 153–159.
- [36] F. De Geuser, W. Lefebvre, F. Danoix, F. Vurpillot, B. Forbord, D. Blavette, Surf. Interf. Anal. 39 (2007) 268–272.
- [37] O.C. Hellman, D.N. Seidman, Mater. Sci. Eng. A 327 (2002) 24–28.
- [38] S.-I. Baik, M. Olszta, S. Brummer, D.N. Seidman, Scripta Mater. 66 (2012) 809–812.
- [39] C. Jiang, D. Sordelet, B. Gleeson, Scripta Mater. 54 (2006) 405–410.